LRP 650/99 November 1999

# Nonstandard Relaxation Oscillations of Magnetically Confined Plasmas

F. Porcelli, C. Angioni, R. Behn, I. Furno,
T. Goodman, M. Henderson, Z.A. Pietrzyk,
A. Pochelon, H. Reimerdes, E. Rossi and O. Sauter

ISSN 0458-5895

# Nonstandard relaxation oscillations of magnetically confined plasmas

F. Porcelli[1,2], C. Angioni[1], R. Behn[1], I. Furno[1], T. Goodman[1], M. Henderson[1], Z. A. Pietrzyk[1], A. Pochelon[1], H. Reimerdes[1], E. Rossi[3] and O. Sauter[1]

[1] *Centre de Recherches en Physique des Plasmas, Association Euratom - Confédération Suisse Ecole Polytechnique Fédérale de Lausanne, Switzerland*

[2] *Istituto Nazionale Fisica della Materia and Dipartimento di Energetica, Politecnico di Torino, Italy*

[3] *Institute for Fusion Studies, University of Texas at Austin, USA*

## Abstract

An experimental account of nonstandard, central magneto-hydro-dynamic (MHD) events in the Tokamak à Configuration Variable (TCV) during localized Electron Cyclotron Resonant Heating (ECRH) is presented. It is shown theoretically that the nonstandard behavior is the consequence of specific features in the electron temperature profile produced by ECRH and by the advection and mixing of electron thermal energy resulting from a resistive MHD instability.

Experimental research on controlled thermonuclear fusion requires the production of hot plasmas with temperatures in the multi-keV range. One effective scheme providing intense localized heating is ECRH [1]. Resonant electromagnetic waves are launched into a magnetically confined plasma, at a frequency matching a low integer multiple of the local EC frequency, $\omega_{ce} = eB/mc$. In recent years, record values of ECRH power density have been attained. This has unveiled new and peculiar plasma behavior. One example is the observation of multipeaked electron temperature profiles and sharp temperature gradients in RTP [2] and TEXT-U [3] experiments, explained in Ref. [4] as the consequence of the interaction between ECRH and resistive magneto-hydro-dynamic (MHD) modes with toroidal n=1 and dominant poloidal m=1 mode numbers. These modes are known to be responsible for the well known internal plasma *sawtooth* relaxation oscillations [5]. In TCV experiments with intense ECRH, sawtooth oscillations acquire a nonstandard character [6] [7]. Nonstandard MHD activity was also observed in T-10 experiments [8]. The purpose of this Letter is to present an experimental account of nonstandard sawtooth behavior in TCV and to provide a theoretical interpretation of the observed phenomena.

TCV is a tokamak with major radius R = 0.89 m, minor radius a = 0.25 m, vacuum vessel elongation $\kappa = 3$ and central magnetic field B = 1.43 T in vacuum. The present ECRH system includes three 82.7 GHz, 500 kW gyrotrons, each with a pulse length of 2 s, for heating at the cyclotron second harmonic resonance via the extraordinary mode. The vertical microwave beam diameter near the plasma center is of order 5 cm, while the horizontal width of the deposition region is O(1 cm). ECRH power densities in excess of $1 \times 10^2$ MW/m$^3$ can be obtained. New insight in the temporal evolution of the different types of MHD modes observed in TCV has become possible thanks to the recently upgraded, 200 channel soft X-ray tomographic system [9], allowing for a sampling time of 13 $\mu s$. The spatial reconstruction of the central emissivity profile is based on a pixel method with characteristic spatial resolution of about 3 cm, to be compared with a typical sawtooth inversion radius of 5-10 cm.

Figure 1 compares standard and nonstandard relaxation oscillations in TCV. Standard

sawteeth, shown in Figs. 1a-c, are observed with auxiliary heating when the ECRH power is deposited on the magnetic axis. Fig. 1a illustrates the plasma equilibrium and wave beam geometry, Fig. 1b presents the line-integrated soft X-ray intensity, $I_X$, for the vertical chord through the plasma center as a function of time and Fig. 1c presents a tomographic reconstruction of the soft X-ray emissivity isocontours.

With off-axis ECRH, different types of nonstandard oscillations are observed [6]. For instance, so called *saturated sawteeth* are often observed when the wave energy is deposited within the magnetic surface where the magnetic winding index, q, equals unity. In this paper, we describe in more detail what happens when the ECRH power is deposited close to the q=1 surface, as shown in Fig. 1d. The line-integrated soft X-ray traces observed in this case have a peculiar shape, shown in Fig. 1e, which suggested the nickname *humpbacks* when they were first observed in the T-10 tokamak [8]. In Fig. 1f we show the corresponding emissivity isocontours. Humpback relaxation oscillations can also be observed with central electron cyclotron (counter)current drive.

For humpbacks and in some cases for saturated sawteeth, the central soft X-ray emissivity is observed to drop and rise on a fast time scale, typically a few hundred microseconds, faster than the heating time, typically a few milliseconds. Thus, the fast rise cannot be attributed to re-heating, but is likely due to the nonlinear development of the m/n=1 instability. For the case of the humpback, a diffusive phase follows, during which the central emissivity is again observed to drop and rise, but on a slow time scale. The overall change in intensity is much smaller for a humpback than for a standard sawtooth for comparable ECRH power, safety factor and total plasma energy content. For instance, in Fig. 1, $\Delta I_x \sim 8\%$ for the humpback and $\sim 25\%$ for the standard sawtooth. The repetition time for humpback relaxations can be significantly longer than the standard sawtooth period.

One way to analyze soft X-ray data is the Singular Value Decomposition (SVD) method [10]. The inverted emissivity measurements form a signal matrix, $X$, which is decomposed into orthonormal spatial eigenvectors $u$ (*topos*) and temporal eigenvectors $v$ (*chronos*), resulting in a separation of variables $X(x,t) = \sum a_k u_k(x) v_k(t)$. The three dominant pairs of

eigenvectors characterizing a humpback oscillation are shown in Fig. 2. The $k = 1$ amplitude, $a_1$, is the largest by two orders of magnitude. For simplicity, only a horizontal cut through the plasma center of the topos is shown. These can be interpreted as follows: $u_1$: average emission profile; $u_2$: peaking or flattening of the average profile; $u_3$: m=1 structure of the emissivity profile. The $k = 1$ chrono oscillates on the time scale of the humpback period. Between subsequent relaxations, the amplitude of the $k = 2$ chrono is nearly constant as compared with its variation during the relaxations, which indicates that the X-ray emissivity does not show the typical peaking of standard sawteeth, but remains nearly flat within the q=1 region. The third pair of eigenvectors shows an m=1 oscillation which significantly exceeds the estimated noise level just before the relaxation phase. The different time behavior of the three eigenvectors suggests that the fast drop and rise of the relaxation phase is due to MHD activity, while the slow oscillation phase is a global phenomenon of the emissivity profile, which can be ascribed to a transport process.

Our theoretical understanding of the humpback phenomenon, in particular of the fast drop-and-rise behavior of the soft X-ray emissivity, is based on the following heuristic picture. When the ECRH power is deposited near the q=1 radius, $r_1$, the temperature profile tends to acquire distinctive features. Specifically, the electron temperature can become relatively flat, perhaps even hollow, in the central region up to the q=1 radius and relatively steep outside this radius, as the result of localized heating and diffusive transport during periods of relative MHD quiescence. These periods are terminated by the onset of m/n=1 magnetic islands [11] [12]. Since the formation of these specific features in the electron temperature profile requires relatively long quiescent periods, improved stability against m/n=1 modes is an important factor. This improvement is possible because ECRH power deposited near the q=1 surface can lead to a reduction of the magnetic shear near that surface (via an increase of the local electrical conductivity), which is known from experiments [13] [14] [15] and theory [16] [17] to produce a stabilizing influence. Clearly, also localized EC current drive can exert a pronounced stabilizing effect, as observed in TCV experiments [18].

Now, let us indicate with $T_0$, $T_1$ and $T_{mix}$ the values of the electron temperature before

the onset of the m/n=1 magnetic island, on the magnetic axis, at the q=1 radius and at the sawtooth mixing radius [11] $r_{mix}$, respectively. This island can grow on a time scale faster than the heating and diffusion time scales. Thus, during the island growth, the temperature on the displaced magnetic axis remains nearly constant, i.e. close to $T_0$. Similarly, the temperature at the island O-point, which corresponds to the flux surface of radius $r_1$ before the onset of the island, remains close to $T_1$. Figure 3a shows the situation when the displacement, $\xi$, of the original magnetic axis is about $0.5r_{mix}$. Since $T_0 \sim T_1$, both the plasma core and the island O-point region are relatively hot. Between these two peaks, a valley in the temperature profile is produced, with a minumum value, $T_{min}$, such that $T_1 > T_{min} \geq T_{mix}$. In fact, the inner and outer legs of the separatrix are in thermal contact, as they are part of the same flux surface cross section, so that magnetic field lines on or near the separatrix connect central plasma regions with regions at a radial distance between $r_1$ and $r_{mix}$ from the center. This valley moves rapidly across the plasma center on the time scale of the island growth, as shown in Fig. 3b. Thus, the plasma temperature at a fixed central point drops and rises quickly during the passage of this valley, reproducing the fast drop-and-rise relaxation phase of a humpback. Note that, starting from a slightly hollow temperature profile peaked at $r_1$ (curve 1 of Fig. 3b), the relaxed profile is peaked on axis (curve 4), as the reconnection process in this case entails a net convection of thermal energy from the q=1 surface to the center. Then, a slow diffusive phase follows, during which the electron temperature on axis slightly drops and recovers as ECRH power is deposited off axis. The case of a standard sawtooth is contrasted in Figs. 3c,d.

Figure 3 is actually the result of a quantitative simulation model, similar to the one proposed in Ref. [4], which solves the thermal energy diffusion equation taking into account the anisotropy introduced by the magnetic field (heat diffusion along magnetic field lines is much faster than cross-field diffusion), a localized electron heat source, plasma rotation and a growing m/n=1 magnetic island. The model is constructed as follows. Since parallel heat diffusion is very large, the temperature is assumed to be constant on magnetic flux surfaces, $T = T(\psi_\star, t)$, where $\psi_\star = \psi_\star(r, \alpha, t)$ is the helical flux function in the presence of an island

with helicity m/n=1 and $\alpha = \theta - \phi$. A suitable model for $\psi_\star$ within the magnetic island, which assumes the specific spatial structure of a resistive internal kink mode [12] in the cylindrical approximation and is consistent with the basic reconnection rules of helical and toroidal flux conservation [11], is given in Ref. [4]. The helical flux function there defined depends on time through the displacement function $\xi(t)$, normalized to the mixing radius, $0 \leq \xi \leq 1$. This model for $\psi_\star$ is consistent with the solution of the ideal MHD equation, $\partial\psi_\star/\partial t + \mathbf{v}\cdot\nabla\psi_\star = 0$, where $\mathbf{v}$ is the velocity field associated with the resistive internal kink mode.

Once the function $\psi_\star$ is so determined, we can write the electron diffusion equation in a Lagrangian frame, i.e. on constant helical flux surfaces. Assuming, for the sake of simplicity, a constant electron density $n$ and a constant cross-field diffusion coefficient, $\chi_\perp$, this equation reads

$$\frac{3}{2}\frac{\partial T}{\partial t} = \chi_\perp(< |\nabla\psi_\star|^2 > \frac{\partial^2 T}{\partial\psi_\star^2} + < \nabla^2\psi_\star > \frac{\partial T}{\partial\psi_\star}) + \frac{< S >}{n}$$

where $S$ is the ECRH heat source and the angular brackets denote flux surface averaging. As a consequence of plasma rotation, the ECRH power is effectively deposited within an annular region comprised between the radii $r_{h1}$ and $r_{h2}$ on the poloidal midplane. We assume, for simplicity, a constant power density within these two radii. This diffusion equation describes the evolution of the temperature on magnetic flux tubes frozen to the plasma flow. At the particular instant in time when two flux surfaces with equal helical flux reconnect, a mixing rule for the thermal energy is implemented [4]. With appropriate boundary conditions, our simulation model is thus specified. However, in this model the function $\xi(t)$ is a free parameter not determined theoretically. Reasonable trial functions for $\xi(t)$ are suggested by stability considerations and may be inferred from experimental data.

Typical simulation results for humpback oscillations are shown in Figs. 3a,b and 4. Input parameters are $r_{h1}/r_1 = 0.85$, $r_{h2}/r_1 = 1.15$, $\chi_\perp\tau_{saw}/r_1^2 = 0.2$ and $P_{EC}\tau_{saw}/(V_1 n) = 3 \times 10^{-16}$J, where $\tau_{saw}$ is the oscillation period, $P_{EC}$ is the ECRH coupled power and $V_1 = 2\pi^2 R {r_1}^2$. For instance, with $\tau_{saw} = 3ms$, $r_1 = 10cm$ and $n = 3 \times 10^{19} m^{-3}$, one obtains

$\chi_\perp = 0.7m^2/s$, a realistic value within the q=1 radius, and $P_{EC} = 500kW$. The function $\xi(t)$ is shown in Fig. 4a. Figure 4b shows the central electron temperature as a function of time. In order to obtain a humpback with our simulation code, one needs to assume heating near the q=1 radius and a relatively long period between successive relaxations during which $\xi(t) \approx 0$, consistently with the experimental indications, so that during the quiescent periods the electron temperature can build up in the region where the heating power is concentrated and $T_1$ can become comparable to or even larger than $T_0$. Figures 4c-d show simulated line integrated soft X-ray traces for two different vertical viewing chords: 4c is from a chord through the center and 4d is from a chord at a distance $0.4r_1$ from the center. The detailed shapes of the line integrated traces depend on the viewing chord.

The simulation results support our heuristic picture of the humpback event and are in good qualitative agreement with the experimental traces. These results are relatively insensitive to small variations of the model input parameters and of the function $\xi(t)$. However, for markedly different choices of parameters, different types of traces can be obtained. In particular, if the ECRH power is deposited well within the q=1 region, we can reproduce saturated as well as triangular sawteeth, depending on the choice of $\xi(t)$. An example of a simulated saturated sawtooth was shown in Ref. [7]. Multi-peaked temperature profiles of the type observed in RTP [2] are obtained with our code assuming narrower ECRH deposition widths and a magnetic island which grows slowly during a large fraction of the time between relaxations.

In conclusion, we have shown that intense localized ECRH can produce nonstandard features in the electron temperature profile, which are the cause of the observed nonstandard sawtooth behavior. Then, the fast drop-and-rise of the soft X-ray line integrated intensity for a humpback is shown to follow the nonlinear development of an m/n=1 magnetic island and the corresponding advection and mixing of thermal energy. The essential aspects of this behavior are captured by our model. The model is also able to reproduce different types on nonstandard sawteeth, such as the saturated sawteeth, as shown in Ref. [7]. However, the model is admittedly very rough and there are many open issues that call for extensions.

One issue relates to current drive effects. Indeed, in general ECRH is accompanied by a small amount of current drive. The sign of the driven current changes according to whether the waves are absorbed above or below the poloidal midplane. Interestingly, the sawtooth behavior was found to be different for top or bottom absorption near q=1 [18], humpbacks being more easily produced with counter current drive. Since current drive modifies the q profile and the local magnetic shear, we expect this to have consequences on the $m/n = 1$ mode stability, which could be taken into account by different choices of the displacement function in our simulation code. Another open issue is the overall detailed shape of a humpback trace. In particular, the slow drop and rise of the soft X-ray emissivity between successive relaxations is most likely the result of transport. Our simulations with constant density and $\chi_\perp$ do show a tendency for the central electron temperature to slowly drop and rise between humpback relaxations, however more accurate modeling requires realistic transport coefficients for the plasma density and thermal energy.

The authors thank Drs. K. A. Razumova and H. Weisen for useful discussions. This work was supported in part by the Swiss NSF and by the Italian CNR.

# REFERENCES


[1] B. Lloyd, *Plasma Phys. Contr. Fusion* **40**, A119 (1998).

[2] N. J. Lopes Cardozo et al, *Phys. Rev. Lett.* **73**, 256 (1994).

[3] G. Cima et al, *Plasma Phys. Contr. Fusion* **40**, 1149 (1998).

[4] F. Porcelli et al, *Phys. Rev. Lett.* **82**, 1458 (1999).

[5] S. von Goeler et al, *Phys. Rev. Lett.* **33**, 1201 (1974).

[6] Z. A. Pietrzyk et al, *Nuclear Fusion* **39**, 587 (1999).

[7] A. Pochelon et al, in *Proc. of the 17th IAEA Fusion Energy Conf.*, Yokohama, Japan, October 1998, paper IAEA-F1-CN-69/EX8/3, to appear in *Nuclear Fusion.*

[8] K. A. Razumova et al, *Plasma Physics Reports* **23**, 13 (1997).

[9] I. Furno et al, in *Proc. 27th EPS Conf. on Contr. Fusion and Plasma Phys.*, Maastricht, 1999, paper P3-031.

[10] T. Dudok de Wit et al, *Phys. Plasmas* **1**, 3288 (1994).

[11] B. B. Kadomtsev, *Fizika Plazmy* **1**, 710 (1975).

[12] B. Coppi et al, *Fiz. Plasmy* **1**, 710 (1976).

[13] R. T. Snider et al, *Phys. Fluids* **B1**, 404 (1989).

[14] F. M. Levington et al, *Phys. Rev. Lett.* **72**, 2895 (1994).

[15] V. P. Bhatnagar et al, *Nuclear Fusion* **34**, 1579 (1994).

[16] F. Porcelli et al, *Plasma Phys. Contr. Fusion* **38**, 2163 (1996).

[17] O. Sauter et al, in *Theory of Fusion Plasmas*, Proc. of the Joint Varenna-Lausanne Int. Workshop, J. W. Connor. E. Sindoni and J. Vaclavik eds. (S.I.F., Bologna, 1998).

[18] T. Goodman et al, *ibid* (Ref. 9), paper P3-040.

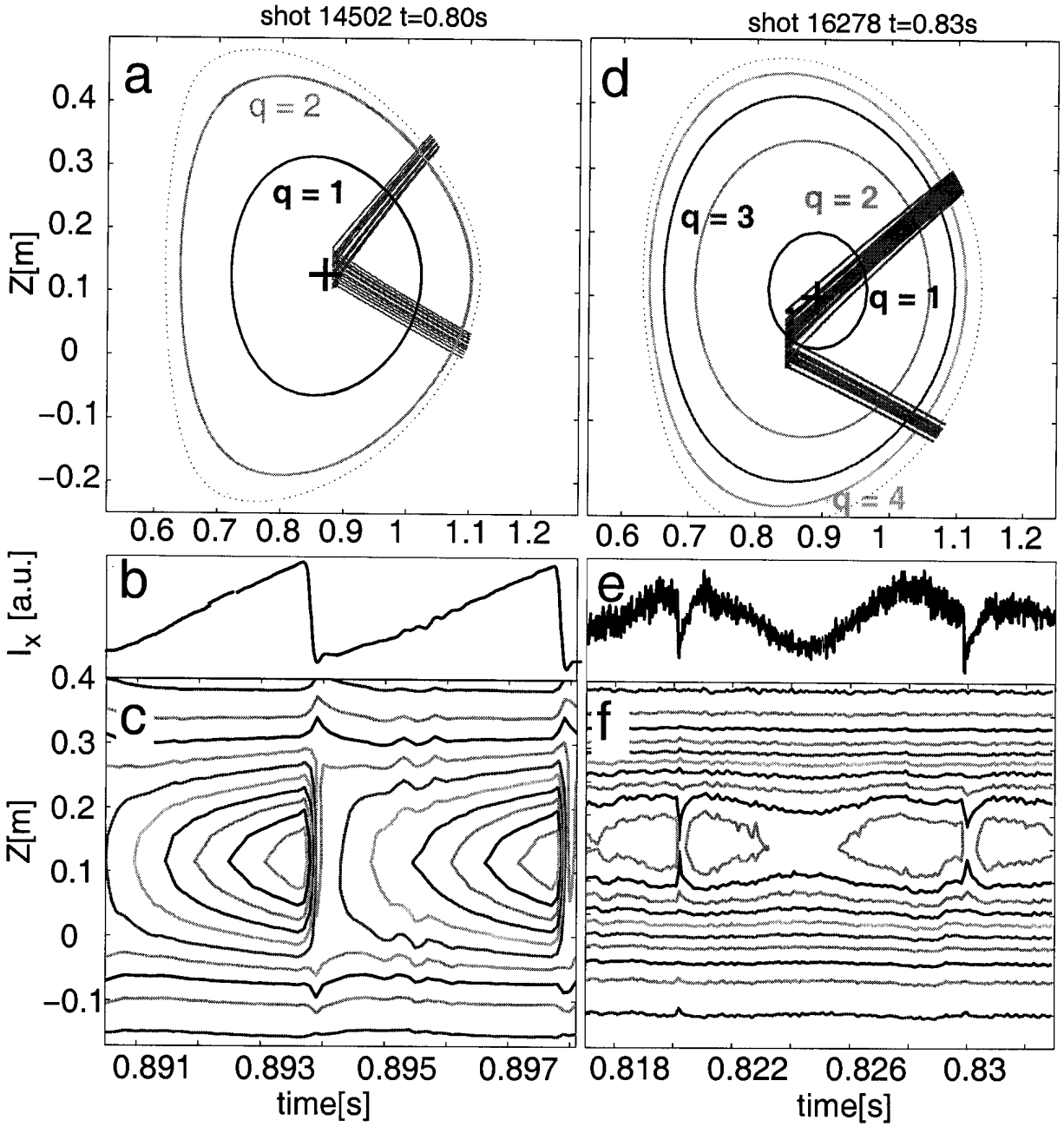


FIG. 1. Standard (a-c) and nonstandard (d-f) central MHD activity in TCV. Frames (a) and (d): poloidal cross sections of equilibrium magnetic flux surfaces and wave beam geometry; (b) and (e): central soft X-ray line integrated intensity as a function of time; (c) and (f): soft X-ray emissivity isocontours.

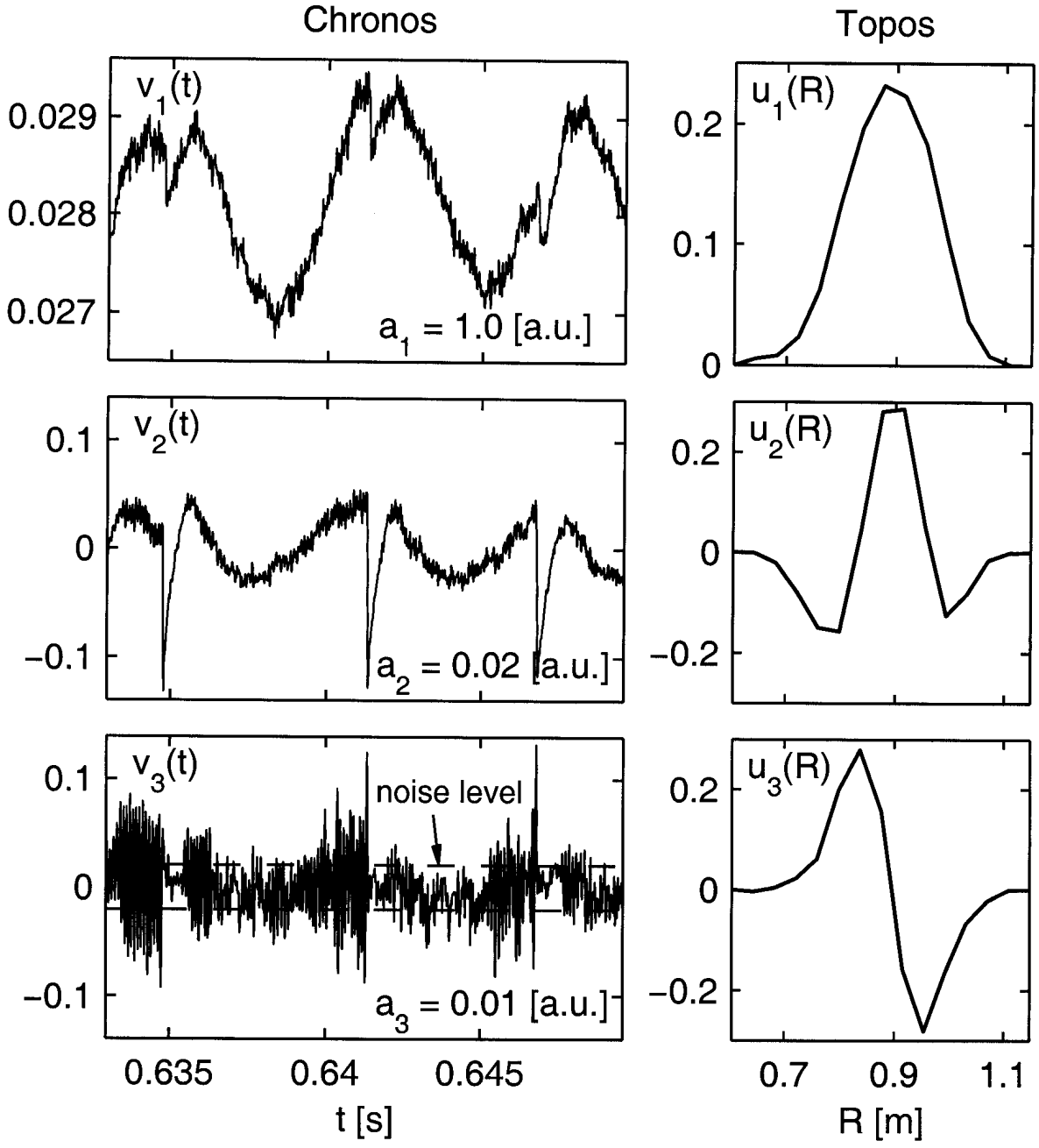


FIG. 2. Singular value decomposition of soft X-ray emissivity for the case of a humpback oscillation.

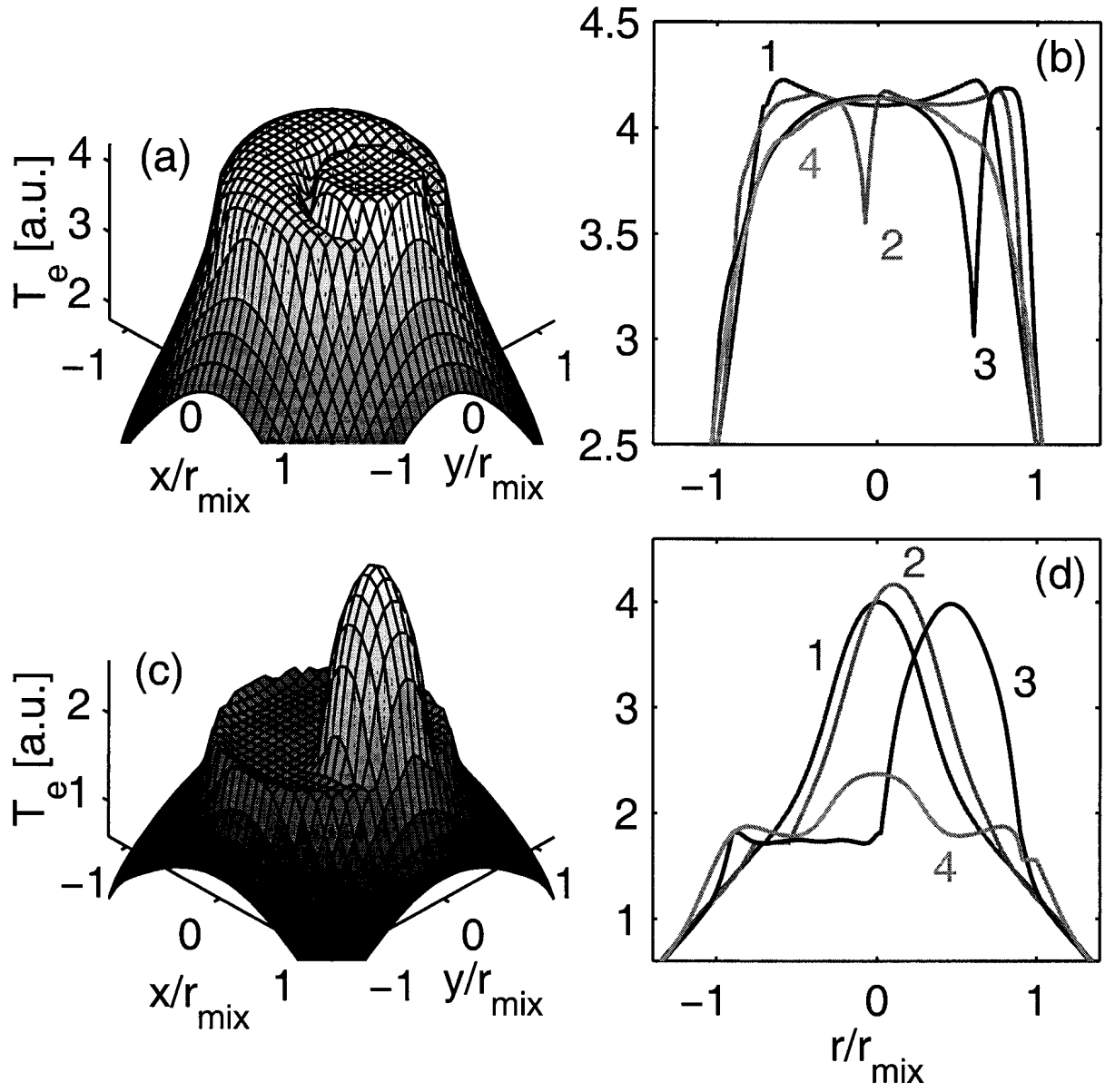


FIG. 3. Simulation results. Humpback relaxation illustrated by (a): the temperature profile at $\xi = 0.53$ and (b): temperature profile sections through the island X and O points at $\xi = 0.14$ (curved marked 1), 0.53(2), 0.9(3) and 1.0(4). Standard sawtooth, illustrated by (c): the temperature profile at $\xi = 0.62$ and (d) sections at $\xi = 0.01(1)$, 0.15(2), 0.62(3) and 0.95(4).

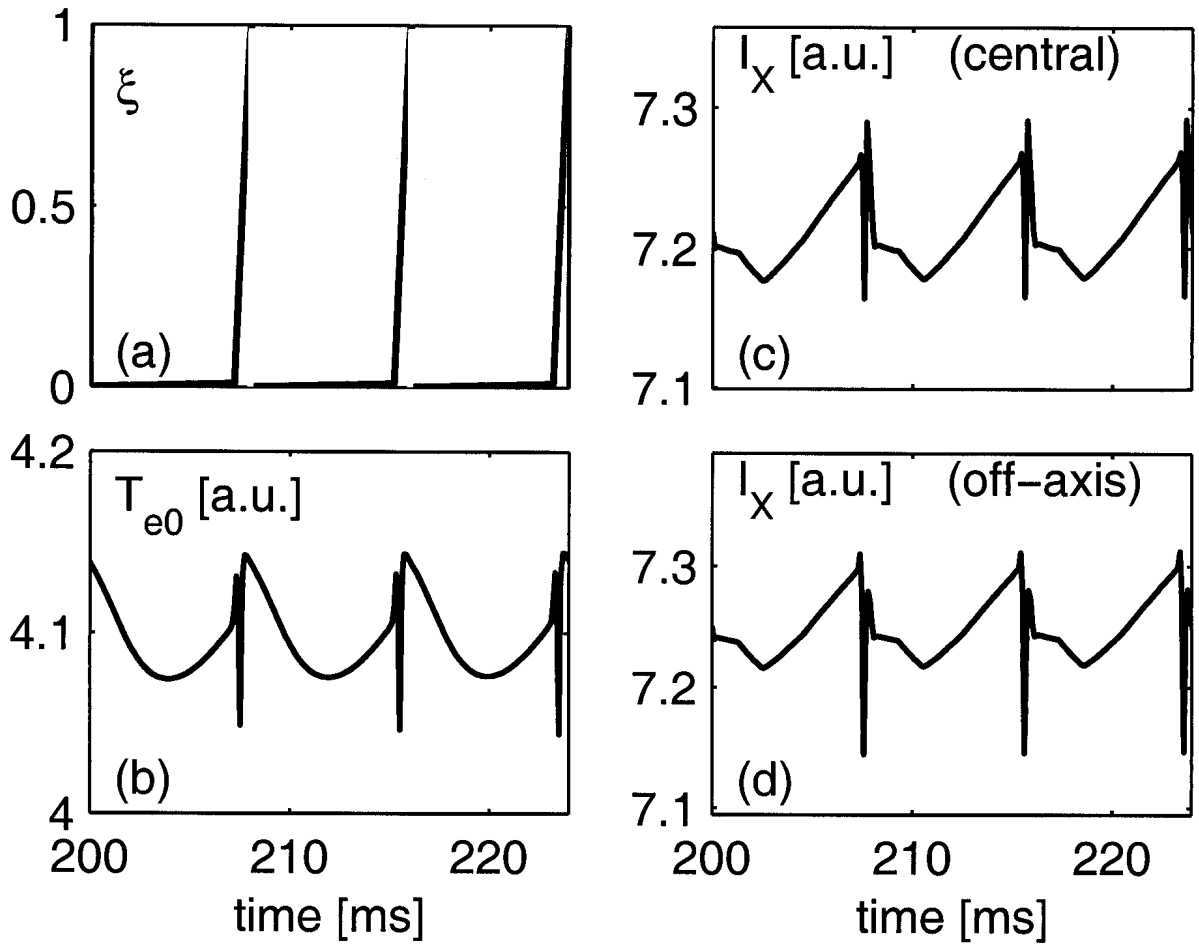


FIG. 4. Simulation results, showing three periods of a humpback relaxation oscillation: (a) $\xi(t)$, (b) central temperature evolution, (c) central and (d) off axis line integrated soft X-ray traces.